AIAA JOURNAL
Vol. 43, No. 12, December 2005

Aeroelastic Model Reduction for Affordable Computational Fluid Dynamics–Based Flutter Analysis

Taehyoun Kim,* Moeljo Hong,† Kumar G. Bhatia,‡ and Gautam SenGupta§
Boeing Commercial Airplane Group, Seattle, Washington 98124-2207

A new approach is presented to generate computational fluid dynamics (CFD)-based reduced-order aerodynamic and aeroelastic models for rapid flutter analysis at an affordable cost. The technique is based on the single-composite-input/eigensystem realization algorithm (SCI/ERA) that has been newly developed at Boeing. Given a large-scaled, discrete-time CFD model whose moving surface boundary is described by multiple structural mode shapes, the SCI/ERA takes time samples of the unsteady response due to a simultaneous excitation of the inputs and identifies the aerodynamic system in terms of low-order matrices. Because the CFD response is sampled almost exclusively for the single representative input this technique can significantly reduce the model construction time. The reduced-order aerodynamic model is coupled with a discrete-time structural model to generate a reduced-order aeroelastic model. For a demonstration of the method, a representative Boeing wind-tunnel airplane modeled by a finite element method and the CFL3D CFD code is studied. It is shown that for the case of 10 structural modes the proposed scheme can reduce the model construction time by a factor of 4–6, yet its unsteady aerodynamic and flutter results are as accurate as those created by other reduction methods.

Nomenclature

$\boldsymbol{A}, \boldsymbol{B}, \boldsymbol{C}, \boldsymbol{D}$	=	aerodynamic system matrices
$\boldsymbol{A}_d$	=	aeroelastic system matrices
$\boldsymbol{A}_s, \boldsymbol{B}_s, \boldsymbol{C}_s$	=	structural system matrices
a	=	angle of attack
b	=	reference length
k	=	reduced frequency, identical to $\omega b/V$
$\boldsymbol{m}, \boldsymbol{c}, \boldsymbol{k}$	=	mass, damping, and stiffness matrices
$\boldsymbol{p}$	=	generalized coordinate vector
q	=	dynamic pressure, identical to $\frac{1}{2}\rho V^2$
R	=	number of chosen singular modes or the dimension of realized model
Re	=	Reynolds number
R_1	=	number of chosen Karhunen–Loeve (KL) modes
T	=	temperature
t	=	real time
$\boldsymbol{u}$	=	input or generalized structural coordinate vector
V	=	freestream speed
$\boldsymbol{x}$	=	state or aerodynamic state vector
$\boldsymbol{y}$	=	output vector
ρ	=	fluid density
τ	=	reduced time, identical to Vt/b
$\boldsymbol{\Phi}$	=	KL modal matrix
ϕ_i	=	KL mode
ω	=	frequency, rad/s
ω_c	=	maximum cutoff frequency

Subscripts

i	=	input
o	=	output
s	=	structure

Presented as Paper 2004-2040 at the AIAA/ASME/ASCE/AHS/ASC 45th Structures, Structural Dynamics, and Materials Conference, Palm Springs, CA, 19–22 April 2004; received 1 June 2004; revision received 13 June 2005; accepted for publication 13 June 2005.

*Principal Engineer, MS 03-KR, Flutter Engineering and Methods Development; taehyoun.kim@pss.boeing.com. Member AIAA.

†Principal Engineer, Enabling Technology and Research.

‡Senior Technical Fellow, Flutter Engineering and Methods Development. Associate Fellow AIAA.

§Principal Engineer, Flutter Engineering and Methods Development. Associate Fellow AIAA.

Introduction

WITH the advent of the modern computational fluid dynamics (CFD) technology, the science and practice of aeroelasticity have evolved into a new stage over the past 25 years. This is particularly true in the transonic and high-angle-of-attack flow regimes where strong nonlinearities involving shock, flow separation, and vortex interaction cannot be modeled by traditional linear aerodynamic theories. See Refs. 1 and 2 for a general overview of recent developments in computational aeroelasticity. As pointed out in Ref. 1, although CFD techniques are becoming a practical tool for solving many static aeroelastic problems, their use in unsteady aeroelasticity is still limited due to the high cost required in the computation of unsteady flow solutions. In CFD, the time it takes to obtain a complete unsteady solution eclipses the time for a static solution to converge. The unsteady calculation is further hampered if multiple flight conditions are to be examined as in typical flutter and dynamic loads surveys for commercial airplanes.

To avoid the excessive computing time encountered during the unsteady calculation, CFD-based reduced-order models (ROMs) have been developed and used. The essence of the aerodynamic ROMs is generalized aerodynamic force (GAF) approach in which unsteady aerodynamic loads due to arbitrary motion are calculated by linear combinations of GAFs obtained for a given set of structural mode shapes. The underlying assumption is that for practical purposes it is sufficient to investigate statically nonlinear, dynamically linear aeroelastic responses. For example, the classical flutter analysis is based on a linear stability theory, and dynamic flight loads calculations practiced at industry do not in general consider large-amplitude behavior of the aircraft. Within this framework, the aerodynamic model should capture the nonlinearities in the steady flow but will only simulate small-amplitude motions around the static position. Once a state-space aerodynamic equation is obtained for the GAFs, it can be combined with a structural equation of motion to yield a reduced-order aeroelastic system. Current techniques that are practiced to produce the unsteady GAFs in the state-space format are the rational function approximation,[3–5] the p-transformation.[6,7] and proper orthogonal decomposition (POD).[8–10] Most recently, based on the input and output time histories from the CFL3Dv6.0 code, aerodynamic ROMs were generated directly in discrete time[11–13] using the eigensystem realization algorithm (ERA).[14]

Unfortunately, all of the available methods pose a serious burden on CPU time and computing resources when the flowfield is driven by multiple structural mode shapes. This is because they are essentially a mode-by-mode approach that produces one set of GAFs per mode. Note that commercial airplanes require as many as 140 structural modes for flutter prediction and 200 modes for dynamic loads calculation and generating aeroelastic ROMs for such an airplane would be extremely time consuming, if not impossible, using the present methods. Therefore, it is imperative to develop a new reduction method that optimizes the model construction time for the multiple inputs and, hence, makes CFD an affordable tool for unsteady aeroelasticity.

The present paper represents an original research effort toward a robust, accurate, and economic model reduction/system identification for unsteady aerodynamic modeling. More specifically, our objective is based on a full-scaled CFD model to construct a discrete-time reduced-order aerodynamic and aeroelastic model in state-space form at an affordable computing cost. To this end, we use the single-composite input/ERA (SCI/ERA) that has been recently developed at Boeing.[15] Given a large-scaled, discrete-time dynamic model with many inputs, the SCI/ERA identifies the system in the state-space form by sampling the system response due to a single representative input, and hence, the model construction time is minimized. This concept of simultaneous excitation was first introduced by Kim[9] and Kim and Bussoletti[10] in a POD-based model reduction. For the construction of the SCI, several types of time signals are considered, including low-pass filtered inputs, a series of impulses, and a series of steps. The reduced-order aerodynamic model is coupled with a discrete-time structural model to generate a reduced-order aeroelastic model. To account for the effect of changes in the freestream speed, the continuous structural model is discretized using varying incremental time steps. For an initial study of the method, the twin-engine transport flutter model (TETFM) modeled by the finite element method (FEM) and CFL3D is considered. It is shown that for the case of 10 structural mode shapes the proposed scheme can reduce the model construction time by a factor of 4–6. It can be expected that the saving factor will increase as more mode shapes are added in the structure. For comparison, the unsteady aerodynamic and flutter results obtained from the present method are compared with those from the traditional ERA (or pulse/ERA) ROM and they are shown to be in a very good agreement.

SCI/ERA Procedure

In this section, the SCI/ERA procedure as applied to the CFD model is summarized. For a full description and discussion of the method, see Kim.[15] The aerodynamic system under consideration is in the following finite dimensional, discrete-time form:

$$\boldsymbol{x}^{n+1} = \boldsymbol{A}\boldsymbol{x}^n + \boldsymbol{B}\boldsymbol{u}^n \tag{1}$$

$$\boldsymbol{y}^n = q(\boldsymbol{C}\boldsymbol{x}^n + \boldsymbol{D}\boldsymbol{u}^n) \tag{2}$$

where $\boldsymbol{x}$ is the aerodynamic state vector, $\boldsymbol{u}$ is the $(N_i \times 1)$ generalized structural coordinate vector, and $\boldsymbol{y}$ is the $(N_o \times 1)$ aerodynamic measurement vector including $(N_i \times 1)$ generalized aerodynamic forces. The equations progress in nondimensional time, $\tau \equiv Vt/b$.

The SCI/ERA starts out by sampling the system pulse responses at the first two time steps, $\tau = 0$ and $\Delta\tau$. They are necessary to identify the input matrices $\boldsymbol{B}$ and $\boldsymbol{D}$. Next, a single set of output samples is taken at $\tau = 0, \Delta\tau, \ldots, M\Delta\tau$ subject to the SCI. For states,

$$\boldsymbol{b}^n_{\mathrm{SCI}} \equiv \sum_{i=1}^{N_i} \boldsymbol{b}_i r_i^n \tag{3}$$

and for outputs,

$$\boldsymbol{d}^n_{\mathrm{SCI}} \equiv \sum_{i=1}^{N_i} \boldsymbol{d}_i r_i^n \tag{4}$$

where r_i^n is identical to a sequence of arbitrary numbers and $\boldsymbol{b}_i$ and $\boldsymbol{d}_i$ are the ith column of $\boldsymbol{B}$ and $\boldsymbol{D}$, respectively. Theoretically, any arbitrary input signals can be used in Eqs. (3) and (4) provided that they are statistically independent. To ensure the independence of the inputs, it is desirable that these time signals be as uncorrelated as possible. After the system state response is obtained by subtracting the pulse responses from the output samples, Hankel-like matrices $\boldsymbol{H}_{c0}$ and $\boldsymbol{H}_{c1}$ are constructed. Finally, the singular value decomposition (SVD) of $\boldsymbol{H}_{c0}$ and psuedoinverting various submatrices generates $\boldsymbol{A}$, $\boldsymbol{B}$, $\boldsymbol{C}$, and $\boldsymbol{D}$, whose dimension R is determined by checking the singular value distribution. Accuracy of the realization is established when the smallest singular value is sufficiently close to zero and one takes all of the linearly independent singular modes, that is, $R = \mathrm{rank}(\boldsymbol{H}_{c0})$. For an accurate realization, one must have a sufficient number of time samples and measurements. If for any reason there are not enough measurements available, one can take extra time samples of the pulse and SCI responses and augment the size of $\boldsymbol{H}_{c0}$ and $\boldsymbol{H}_{c1}$ (Ref. 15).

When the SCI is applied to a time-accurate, fully nonlinear CFD model, the following must be considered. First, one must use time inputs that are as smooth as possible so that the CFD code can converge within a reasonable number of subiterations, preferably in the range of 10–20. Otherwise, a large number of subiterations must be employed to minimize residual errors in the samples, which inevitably increases the computing time. Second, caution must be taken not to excite the inherent nonlinearities in the code when extracting the GAFs. Applying a large amplitude will not only violate the assumption behind Eqs. (1) and (2) but will also nullify the principle of superposition on which the SCI is based. Usually, injecting a very small amplitude on the order of magnitude 10^{-3} suppresses the nonlinearity, but it could depend on a specific flight condition and the nature of the mode shapes. Third, it is desirable to come up with a strategic scheme to excite only the lowest frequency content in the CFD response. This is because aeroelastic responses are dominated by the structural eigenmodes whose natural frequencies are much lower than the frequency content of the CFD model, and hence, unoptimized CFD responses will result in aeroelastic models of unnecessarily large sizes.[15]

Time Signals for Simultaneous Excitation

A few candidate signals for the SCI are considered in this section. Note that for an ideal linear model any of these SCIs can be used and all of them should yield ROMs of essentially the same quality. However, there are obviously merits and demerits in each SCI when applied to nonlinear CFD codes, and as such, care must be exercised when selecting the signals.

Random-Signal-Based SCI

It is natural to use random signals for construction of SCI. That is, use r_i^n as identical to a sequence of random numbers in Eqs. (3) and (4). For our reference, we will label this type as random-signal-based SCI (RSCI). Figure 1 shows three sets of random numbers generated using MATLAB®. Unfortunately, for such a sharp, rapidly changing input, the CFL3D code requires a very large number of subiterations to achieve a moderate rate of convergence especially in the critical low-frequency range and, hence, a very long computing time overall. For this reason, random signals are not in general recommended.

Filtered-Signal-Based SCI

To inject smooth inputs to CFD, one can filter the random signals through a low-pass filter. That is,

$$r_i^n = r_{fi}^n \tag{5}$$

where r_i^n is identical to a sequence of filtered random numbers. Using the low-frequency signals will allow better convergence in the CFD solutions. Furthermore, because the frequency content is limited, it is possible to generate a smaller ROM directly from the SCI/ERA without any further reduction. A potential drawback is that if the filtered signals become too narrowly banded, they may

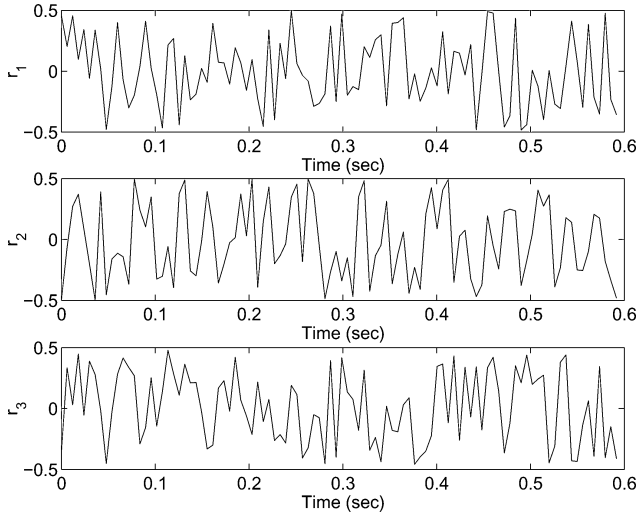

Fig. 1 Statistically independent random signals.

not be as uncorrelated as desired. However, based on the theory of ergodicity,[16] the statistical independence could be fortified by using longer signals and sampling the response for a longer period of time. This type is labeled filtered-signal-based SCI (FSCI).

Step-Signal-Based SCI

In analogy to a single-step input, one can apply multiple step inputs in a sequential manner,

$$r_i^n = u_i^{n-k_i} \tag{6}$$

where r_i^n is identical to a step input applied at k_ith step and where

$$u_i^{n-k_i} \equiv \begin{cases} 0, & n = 1, 2, \ldots, k_i - 1 \\ 1, & n \geq k_i \end{cases} \tag{7}$$

To assure independence of the inputs, the onsets of the signals must be apart from each other by a sufficient number of steps, that is, k_i must be large enough. Unlike the RSCI, convergence is normally established after each step has been applied for step-signal-based SCI (SSCI).

Pulse-Signal-Based SCI (PSCI)

One can also apply multiple pulse inputs in a sequential manner,

$$r_i^n = \delta_i^{n-k_i} \tag{8}$$

where r_i^n is identical to a step input applied at k_ith step and where

$$\delta_i^{n-k_i} \equiv \begin{cases} 1, & n = k_i \\ 0, & n = \text{all other points}) \end{cases} \tag{9}$$

for pulse-signal-based SCI (PSCI). Again, k_i must be large enough to guarantee independence of the applied signals. Because only one sharp pulse is involved for each input, usually a good convergence is maintained. However, its overall performance and accuracy are not as robust as the SSCI.

Second Reduction Based on Frequency-Domain Karhunen–Loeve/SCI Method

When sharp signals, such as the SSCI or PSCI are applied, they will excite all of the system dynamics. As a result, the frequency range of the original system, $(0, \pi/\Delta t)$, will be preserved in the ROM. Because the structural mode shapes have natural frequencies much lower than this upper limit, given the highest frequency of interest for aeroelastic applications, ω_c, one will find that $\omega_c \ll \pi/\Delta t$. Therefore, the aerodynamic ROM produced by the SCI/ERA can be further reduced by the frequency-domain Karhunen–Loeve (FDKL) method (see Ref. 17). In this method, a set of optimal modes $\boldsymbol{\Phi}$ are obtained by sampling frequency samples of the SCI/ERA ROM. Again, the SCI is used to excite the multiple inputs concurrently, but this time r_i^n are random numbers prescribed in the frequency domain.[18] After the KL modes are obtained, the ROM matrices are reduced via Galerkin's approximation yielding a new ROM,

$$\boldsymbol{p}^{n+1} = \boldsymbol{A}_1 \boldsymbol{p}^n + \boldsymbol{B}_1 \boldsymbol{u}^n \tag{10}$$

$$\boldsymbol{y}^n = q\left(\boldsymbol{C}_1 \boldsymbol{p}^n + \boldsymbol{D}\boldsymbol{u}^n\right) \tag{11}$$

where

$$\boldsymbol{x} \simeq \boldsymbol{\Phi}\boldsymbol{p} \tag{12}$$

$$\boldsymbol{\Phi} \equiv \begin{bmatrix} \phi_1 & \phi_2 & \cdots & \phi_{R_1} \end{bmatrix} \tag{13}$$

$$\boldsymbol{A}_1 \equiv \boldsymbol{\Phi}^T \boldsymbol{A} \boldsymbol{\Phi} \tag{14}$$

$$\boldsymbol{B}_1 \equiv \boldsymbol{\Phi}^T \boldsymbol{B} \tag{15}$$

$$\boldsymbol{C}_1 \equiv \boldsymbol{C}\boldsymbol{\Phi} \tag{16}$$

The dimension of the new model is $(R_1 \times R_1)$, which is equal to the rank of the KL covariance matrix and is smaller than R (Ref. 15).

Aeroelastic ROM Based on CFD ROM

A structural model is normally described in real, continuous time,

$$\boldsymbol{m}\ddot{\boldsymbol{u}} + \boldsymbol{c}\dot{\boldsymbol{u}} + \boldsymbol{k}\boldsymbol{u} = \boldsymbol{y} \tag{17}$$

where $\cdot$ and $\cdot\cdot$ represent the first and the second derivatives with respect to t, respectively. To construct the aeroelastic model, the continuous-time equation (17) is discretized in time,

$$\boldsymbol{z}^{n+1} = \boldsymbol{A}_s \boldsymbol{z}^n + \boldsymbol{B}_s \boldsymbol{y}^n \tag{18}$$

$$\boldsymbol{u}^n = \boldsymbol{C}_s \boldsymbol{z}^n \tag{19}$$

where

$$\boldsymbol{z} \equiv \begin{Bmatrix} \boldsymbol{u} \\ \dot{\boldsymbol{u}} \end{Bmatrix} \tag{20}$$

$$\boldsymbol{C}_s \equiv [\boldsymbol{I} \quad \boldsymbol{0}] \tag{21}$$

The reduced-order aeroelastic model can be obtained by combining the aerodynamic ROM given by Eqs. (1) and (2) or (10) and (11) and the structural model, Eqs. (18) and (19),

$$\boldsymbol{X}^{n+1} = \boldsymbol{A}_d \boldsymbol{X}^n \tag{22}$$

where

$$\boldsymbol{A}_d \equiv \begin{bmatrix} \boldsymbol{A} & \boldsymbol{B}\boldsymbol{C}_s \\ q\boldsymbol{B}_s\boldsymbol{C} & \boldsymbol{A}_s + q\boldsymbol{B}_s\boldsymbol{D}\boldsymbol{C}_s \end{bmatrix} \tag{23}$$

Although q can change in Eq. (23), if the structural model is discretized using a fixed incremental time step, the aeroelastic ROM cannot be used at speeds other than V_{ref} for which the CFD samples were taken. Therefore, to account for the effect of changing the freestream speed, it is necessary to adjust the incremental time step according to $\Delta t = \Delta\tau b/V$ for the varying speed V and discretize the structural model accordingly.[15]

Once the aeroelastic ROM [Eq. (22)] is constructed, various aeroelastic analyses such as flutter analysis and transient simulation can be performed conveniently. In particular, for the flutter check we have developed the discrete-time eigenanalysis and mode tracking method.[18] In this technique, aeroelastic sensitivity matrix of the state-space equation (23) at the current dynamic pressure $q = \frac{1}{2}\rho V^2$ is calculated and changes in the aeroelastic eigenmodes at the next dynamic pressure level, $q + \Delta q = \frac{1}{2}(\rho + \Delta\rho)(V + \Delta V)^2$, are predicted and can be corrected using an iterative method. This results in a V–g plot where damping and frequency of the structural modes are plotted as functions of the dynamic pressure.

Limitations of Aeroelastic ROM

The aeroelastic equation of motion (22) has two independent variables, the fluid density ρ and the freestream speed V. This allows one to rely on the classical V–g analysis where the damping and frequency of structural modes are plotted as functions of the dynamic pressure, or equivalently, the speed and density. Strictly speaking, when a Navier–Stokes CFD code is used, the aerodynamic and aeroelastic ROMs are valid only for the flow condition at which the CFD time history samples were taken. The unsteady flowfield is a complicated, nonlinear function of a flow parameters such as Mach number, density, speed, viscosity, temperature, angle of attack, and so on, so that it cannot be extrapolated beyond the present condition in a simple analytical manner. Therefore, to benefit the V–g analysis based on the aeroelastic ROM, one has to make assumptions about the flowfield, especially the following:

1) Mach number does not change.

2) At the fixed Mach number, the effects of changing freestream Reynolds number, temperature, and pressure are negligible.

3) At the fixed Mach number, the effect of changing static aeroelastic deformation from one dynamic pressure to another is negligible.

With these assumptions, one can produce the so-called matched-point solutions using the flutter analysis.

Despite the inherent limitations in the ROMs, once they are constructed, aeroelastic analyses and simulations can be executed in a negligible amount of time. Apart from this obvious advantage, the aeroelastic ROMs have the following additional merits. First, by changing dynamic pressure values in the equations one can easily modify the ROMs to cover flow conditions far apart from the reference condition, these new conditions being best approximated when they are not too far apart from the reference one. Second, the small model size makes it possible to perform active control system design, optimization, and various parametric studies directly based on the models.

TETFM Based on CFL3D

Wind-Tunnel Model

Figure 2 shows the TETFM wind-tunnel layout. Details of the model may be found in Ref. 19. The TETFM was tested multiple times to study various aerodynamic aspects in the early 1980s and 1990s at the NASA Langley Research Center Transonic Dynamics Tunnel (TDT).

Computational Model

The original computational model of TETFM contains a full wing–body–strut–nacelle configuration. However, in this paper, a simplified model was used to demonstrate the newly developed approach. The model is referred to as wing–pencil–nacelle (WPN), and only the wing is modeled aerodynamically (Fig. 3). The mass of the nacelle was included in the FEM model. Thus, the structural mode shapes (on the wing), the mass, and stiffness matrices of the two configurations are identical to those of the original model. Another difference is that the outer mold line (OML) of the WPN wing was based on cruise wing shape instead of the customary jig shape (the shape of the wing as built in the tooling). Because a wall-function formulation was used for the turbulence modeling, the minimum normal distance was set to obtain $60 < y+ < 500$. The reference area, mean aerodynamic chord, and half-span were 2248 in.^{2} (1.45 m^2), 24 in. (0.61 m), and 93 in. (2.36 m), respectively. The grid has approximately 700,000 cells and 30 blocks. A characteristics inflow–outflow boundary condition is used for far-field condition.

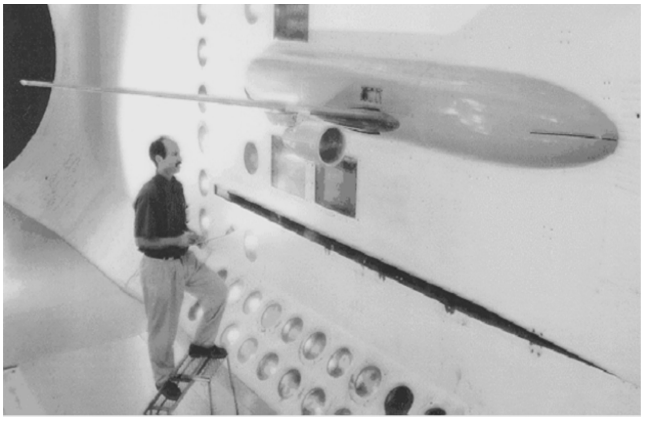

Fig. 2 TETFM in TDT.

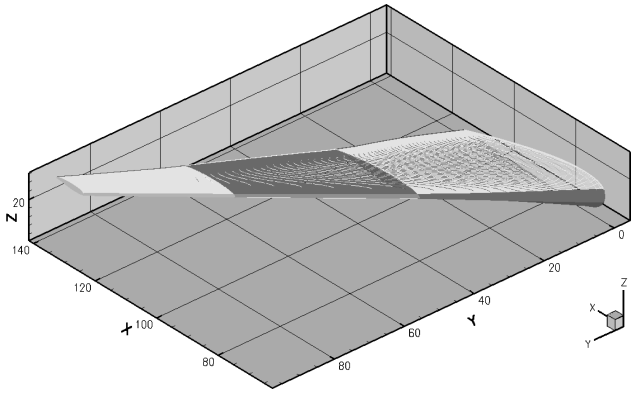

Fig. 3 CFL3D grids for WPN model.

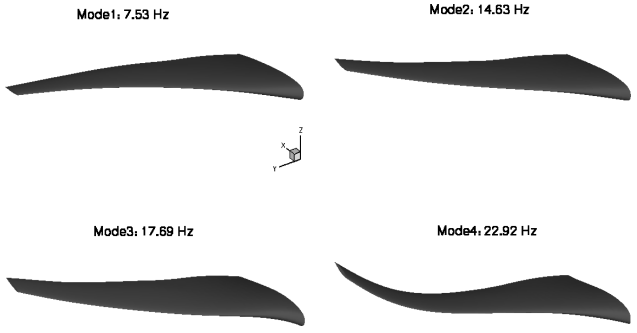

Fig. 4 First four structural mode shapes for WPN model.

Mode Shapes

The mode shapes were derived from an Elfini FEM model using Boeing's in-house interpolation process. Only the first 10 modes are included in the calculations for the demonstration of the current approach. Figure 4 shows the first four mode shapes. The vertical dimension was expanded a by factor of five for clarity. The structural mode shape natural frequencies range from 7.55 to 66.15 Hz.

Results and Discussion

For the demonstration and verification of the proposed method, aerodynamic and aeroelastic ROMs of the WPN configuration modeled by CFL3Dv6.0 code were obtained based on the SCI/ERA. The reference flow condition for which all of the CFL3D solutions were obtained is summarized as follows: medium = R134a, $M = 0.831$, $a = -2$ deg, $q = 149$ psf, $Re = 2.7 \times 10^6$/ft, and $T = 530^\circ$R. This condition corresponds to a preflutter point close to the first flutter instability (hump mode). After a static solution converged, a single set of GAF time histories due to a SCI was obtained. Along with the SCI response, aerodynamic responses due to the individual modes in the form of step signals were calculated at the first two time steps. Unless indicated otherwise, all of the unsteady CFL3D calculations were executed using 995 time steps and 15–20 subiterations. Because the 10 GAFs were the only outputs available from CFL3D, to augment the size of the output matrix it was necessary to sample the step responses at 79 additional time steps beyond the first two steps. Thus,

the total number of samples used in the system identification was 1805. Note that in Ref. 13, 995 samples were taken for each mode, totaling 9950 steps altogether. All of the CFL3D runs were submitted on an IBM Regatta machine using a single domain and a single CPU, that is, without parallel computing for multiple domains.

For the simultaneous excitation, two of the inputs mentioned earlier, the FSCI and SSCI, were used. It was found that even after 50 subiterations in each time step the RSCI did not produce good GAFs, especially in the low-frequency region. The PSCI produced better GAFs, but again their low-frequency spectrum was not robust enough to generate accurate ROMs. For these reasons, no results obtained from the RSCI and PSCI are reported here. To avoid exciting nonlinearities, the maximum amplitudes in all of the inputs were restricted to 0.001. In the postsignal processing, the 10 step responses were deconvoluted to produce system pulse responses, which, along with the SCI output response, resulted in (810×914) Hakel-like matrices, $\boldsymbol{H}_{c0}$ and $\boldsymbol{H}_{c1}$. After the SVD of $\boldsymbol{H}_{c0}$ was obtained and the singular values were checked, the matrix algebra outlined in Ref. 15 produced reduced-order system matrices $\boldsymbol{A}$, $\boldsymbol{B}$, $\boldsymbol{C}$, and $\boldsymbol{D}$.

FSCI/ERA ROM

The first case is FSCI/ERA ROM. This label refers to a ROM obtained by SCI/ERA using an FSCI. To prepare an FSCI, (995×10) arrays of random signals were filtered using a low-pass filter with a cutoff frequency of 318 Hz (Fig. 5). Note that this frequency is approximately five times lower than the maximum frequency in the CFL3D model, $\pi/\Delta t = 1496$ Hz. The time marching within CFL3D for this input was executed using 20 subiterations per each time step. To study the effect of the filtering on the ROM, another set of arrays consisting of (1327×10) random numbers was also filtered using a cutoff frequency of 159 Hz (Fig. 6). For this FSCI, the number of time steps was increased from 995 to 1327 to compensate for possible degradation in the statistical independence that might result from the lower cutoff frequency of the new filter. However, when it is considered that the new signal is twice as smooth as the first FSCI and, hence, will converge faster, the number of subiterations was decreased from 20 to 15. As a result, the total number of subiterations were 19,900 and 19,905, respectively, and hence, the total computational costs were about the same in the two cases. The SVD of the Hankel-like matrices $\boldsymbol{H}_{01}$ of the resulting FSCI responses yielded (60×60) and (68×68) system matrices, respectively. It is noted that these numbers represent the largest dimensions of the system matrices for which their eigenvalues remain stable and all of the lightly damped fluid modes stay within $(-\boldsymbol{\omega}_c, \boldsymbol{\omega}_c)$. Figures 7 and 8 are eigenvalue plots of the aerodynamic ROMs. Note that the eigenvalues are indeed stable and the frequency spectrum of the plots approximately coincide with $(-318, 318)$ and $(-159, 159)$ Hz, respectively, the frequency bandwidths of the two FSCIs used. For comparison, a ROM based on the pulse/ERA was also obtained using 10 individual pulse responses. The pulse responses here were obtained by deconvoluting 995 samples of step responses with 15 subiterations. Initially, a stable (512×512) system matrix was constructed using the method. It was then reduced further by the FDKL/SCI to (104×104) using a cutoff frequency of 71.6 Hz, an upper bound to the natural frequencies of the structural modes.

Figures 9 and 10 show several GAFs obtained from the ROMs (FSCI/ERA ROM 1 and 2) in the time domain. Also presented for

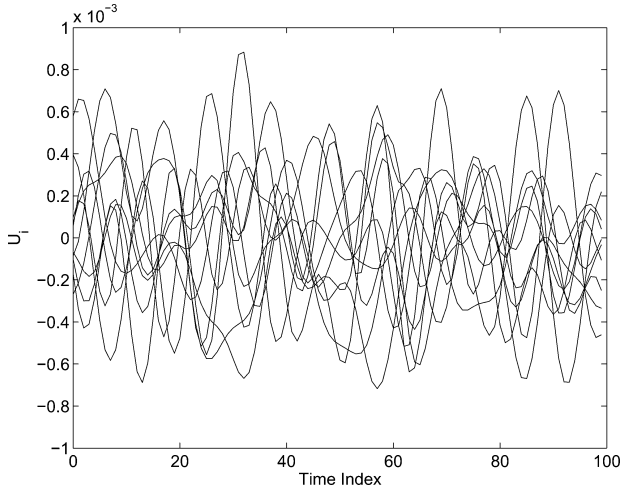

Fig. 5 FSCI 1 10 filtered signals, $\omega_c = 318$ Hz.

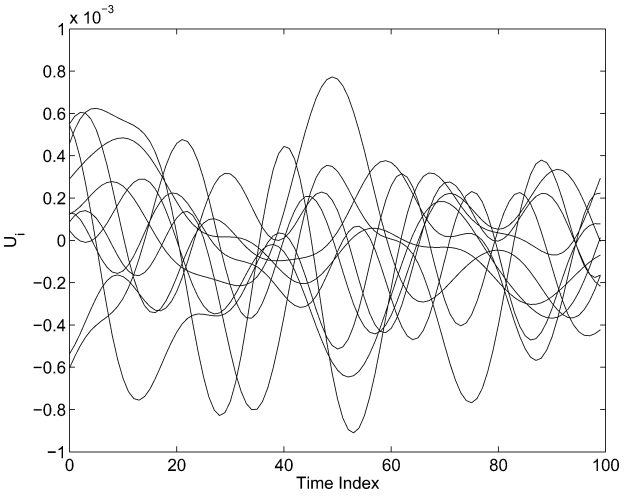

Fig. 6 FSCI 2 10 filtered signals, $\omega_c = 159$ Hz.

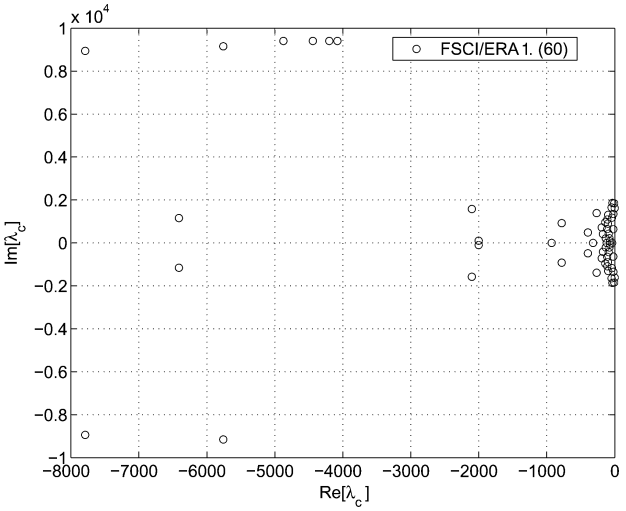

Fig. 7 Aerodynamic eigenvalues: FSCI/ERA 1 (60×60), $\omega_c = 318$ Hz.

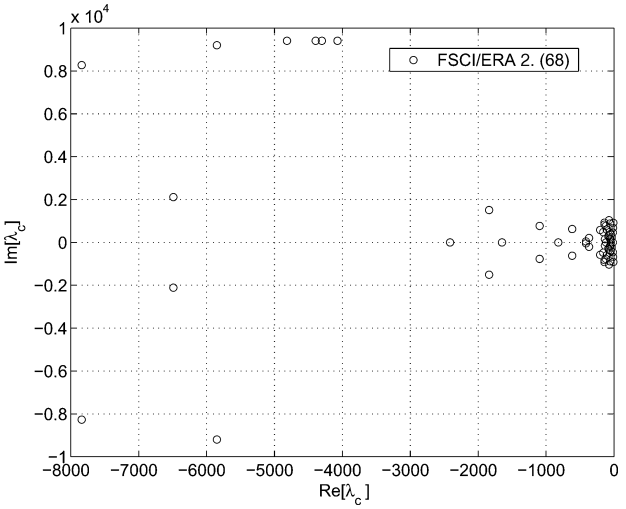

Fig. 8 Aerodynamic eigenvalues: FSCI 2 (68×68), $\omega_c = 159$ Hz.

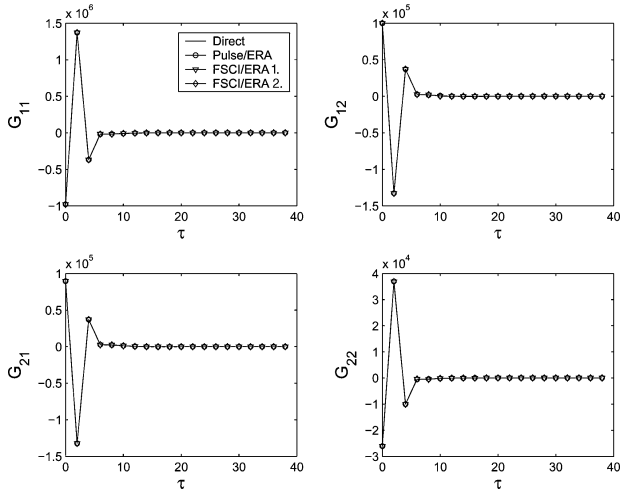

Fig. 9 GAFs: FSCI/ERA 1 vs FSCI/ERA 2, $0 < \tau < 38$.

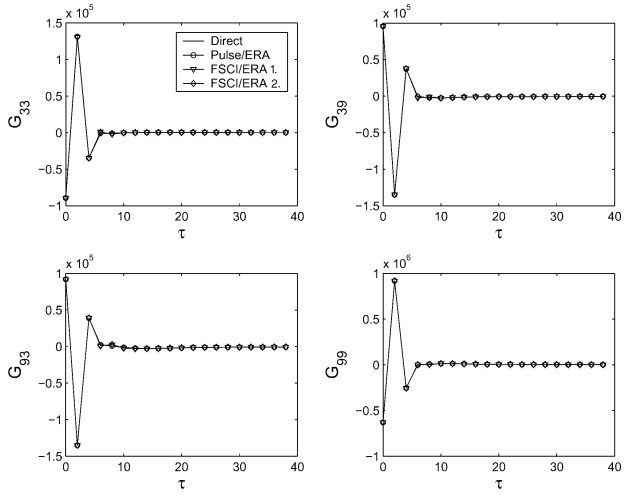

Fig. 10 GAFs: FSCI/ERA 1 vs FSCI/ERA 2, $0 < \tau < 38$.

comparison are the GAFs generated using the pulse/ERA ROM and the direct impulse solutions. As can be seen from Figs. 9 and 10, the four sets of the curves match very well. Based on these results alone, it is tempting to conclude that the SCI/ERA has created excellent aerodynamic ROMs based on the FSCIs. However, Figs. 9 and 10 do not reveal much information about low-frequency behavior of the ROMs, which is critical in aeroelastic applications. In Figs. 11 and 12, the same GAFs were reproduced in the frequency domain for the range of $0 < k < 0.075$, or equivalently, $0 < f < 71.6$ Hz. Also shown in Figs. 11 and 12 are the GAFs from the direct solutions that were obtained by fast Fourier transform of the 995 pulse response samples. It is seen that although G_{22} of the FSCI/ERA ROM 1 shows some degradation, overall the frequency responses compare well. However, the accuracy of the ROMs in the frequency domain is not as good as in the time domain. This result is consistent with the findings in Ref. 11.

Figures 13 and 14 are the V–g plots of the two ROMs as the dynamic pressure increases from 0 to 300 psf. In the calculation of the aeroelastic modes, to be consistent with the wind-tunnel test only the density of the freon gas medium was changed, whereas the tunnel speed was fixed at the reference value, 414.67 fps. In general, there is a good match in both the growth rate and frequency curves (Fig. 13) between the different ROMs. According to the FSCI/ERA ROM 1, the first flutter instability occurs at $q = 156.3$ psf, whereas the second instability (tip mode) is at $q = 248.4$ psf. The FSCI/ERA ROM 2 predicts the instabilities at 149.8 and 248.4 psf, respectively. On the other hand, the pulse/ERA ROM yields the flutter points at 152 and 250.8 psf, respectively. Therefore, the first ROM has 2.83 and

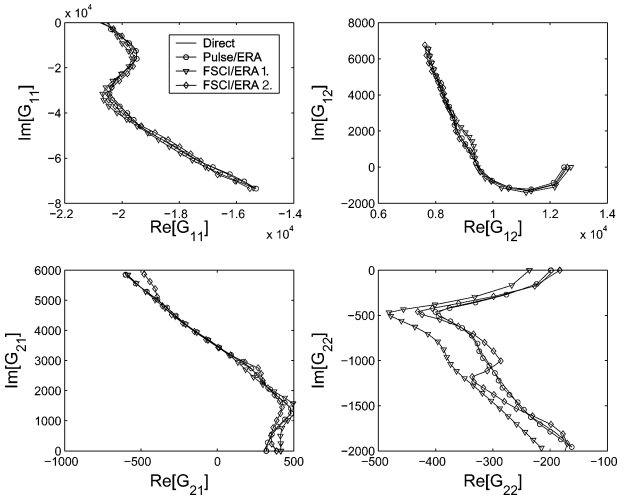

Fig. 11 GAFs: FSCI/ERA 1 vs FSCI/ERA 2, $0 < k < 0.075$.

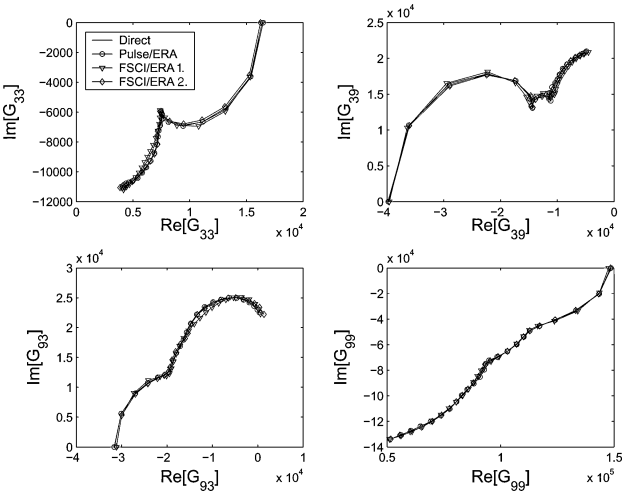

Fig. 12 GAFs: FSCI/ERA 1 vs FSCI/ERA 2, $0 < k < 0.075$.

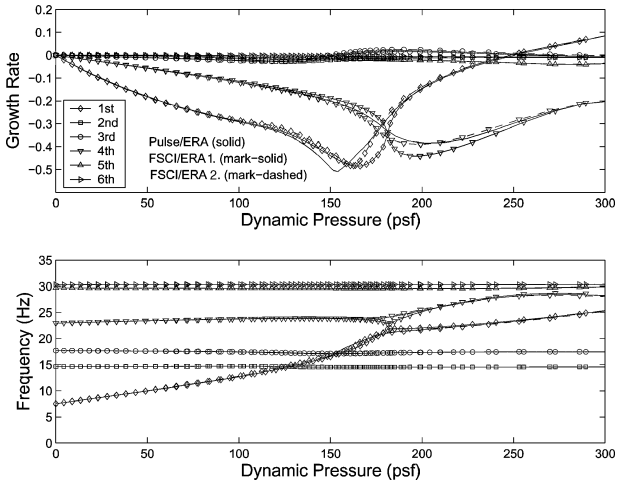

Fig. 13 V–g plot: FSCI/ERA 1 vs FSCI/ERA 2.

0.96%, whereas the second ROM has 1.45 and 0.96% differences with respect to the pulse/ERA ROM in predicting the flutter points.

SSCI/ERA ROM

The next case is SSCI. The SSCI was constructed using a series of step inputs of magnitude 0.001 (Fig. 15). The first step input starts at $t = 0$, and the subsequent signals were delayed by 80 steps from previous ones. After the last step input was introduced at the 721st step, all of the 10 inputs were held at the constant level for

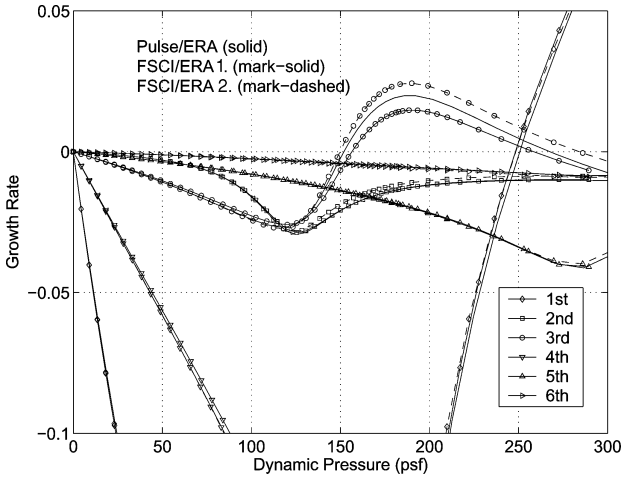

Fig. 14 V–g plot: FSCI/ERA 1 vs FSCI/ERA 2 (growth rate only).

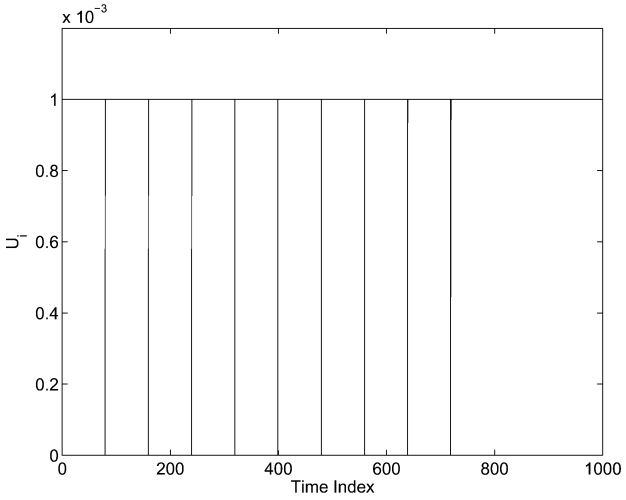

Fig. 15 SSCI 10 step signals.

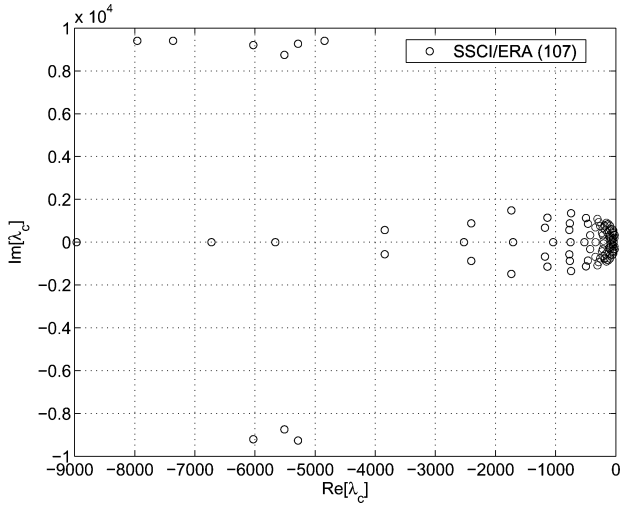

Fig. 16 Aerodynamic eigenvalues: SSCI/ERA (107 × 107).

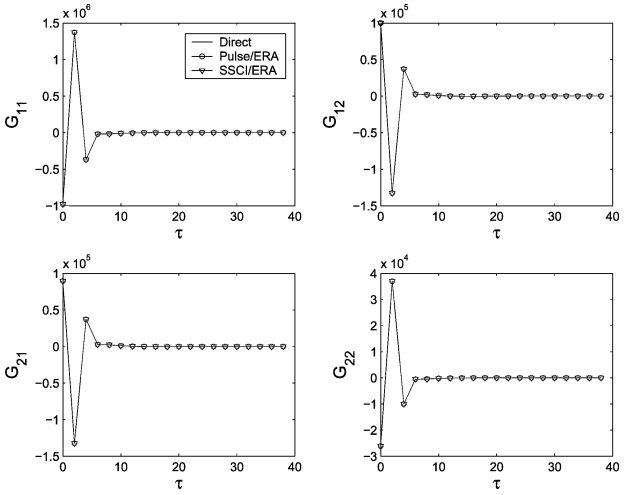

Fig. 17 GAFs: SSCI/ERA, $0 < \tau < 38$.

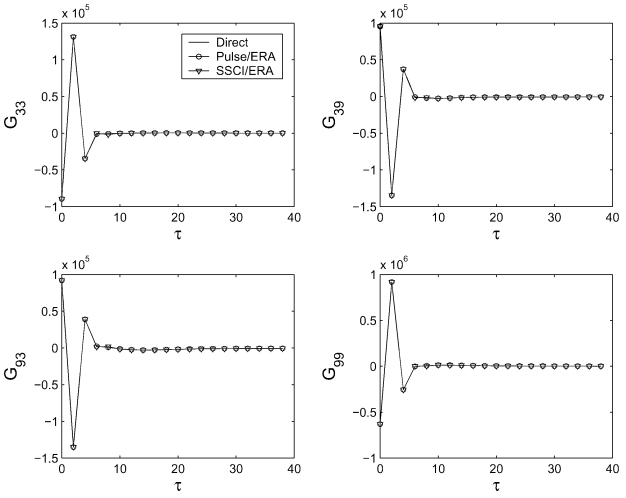

Fig. 18 GAFs: SSCI/ERA, $0 < \tau < 38$.

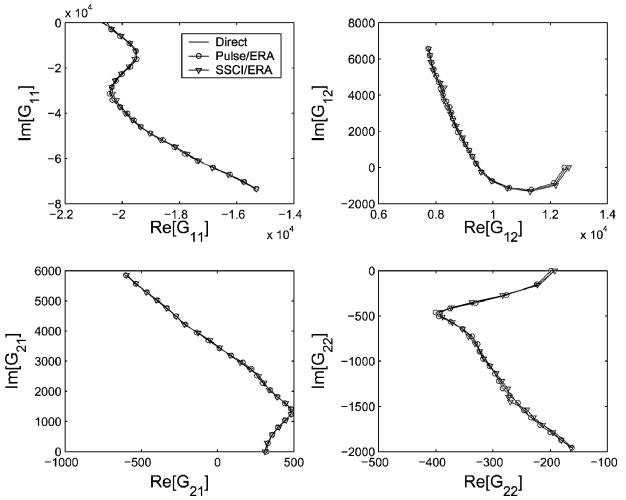

Fig. 19 GAFs: SSCI/ERA, $0 < k < 0.075$.

additional 274 steps. Thus, the total number of steps in the SSCI is 995. The time marching was executed using 15 subiterations. After a stable (512×512) system matrix was obtained from the SCI/ERA procedure, it was further reduced based on the FDKL/SCI to (107×107) using the cutoff frequency 71.61 Hz. Figure 16 shows the eigenvalue spectrum of the resulting ROM. Figures 17–20 show GAFs of the SSCI/ERA ROM in the time and frequency domains, respectively. Unlike in the earlier ROMs, there is an excellent match throughout between the new ROM and the pulse/ERA ROM both in the time and frequency domains. A possible contribution to this high level of accuracy is that the same step signals were used both in the individual and simultaneous excitations, and as a result, the samples required in the SCI/ERA process must have been generated in a highly consistent, accurate manner. Thus, the SCCI/ERA ROM predicted the two flutter points at 152.2 and 249.9 psf, which are within only 0.13 and 0.36% differences from the predictions made by the pulse/ERA ROM (Figs. 21 and 22).

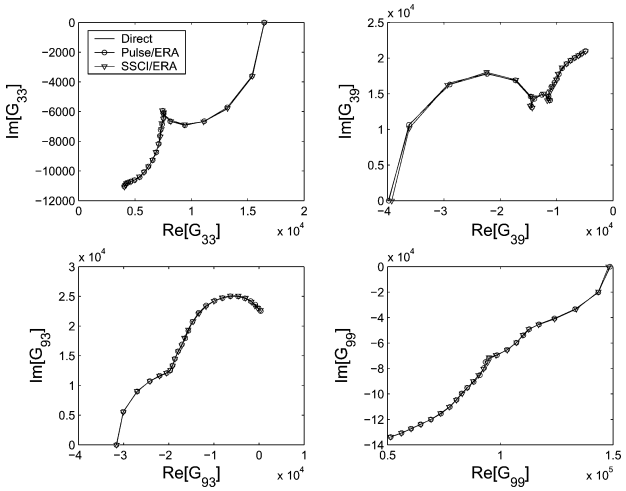

Fig. 20 GAFs: SSCI/ERA, $0 < k < 0.075$.

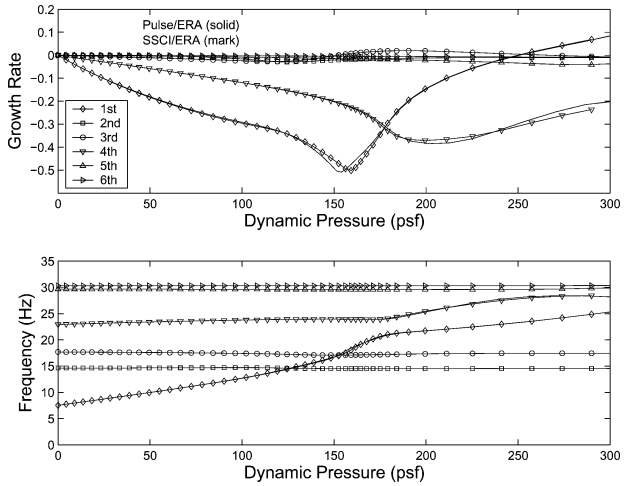

Fig. 21 V–g plot: SSCI/ERA.

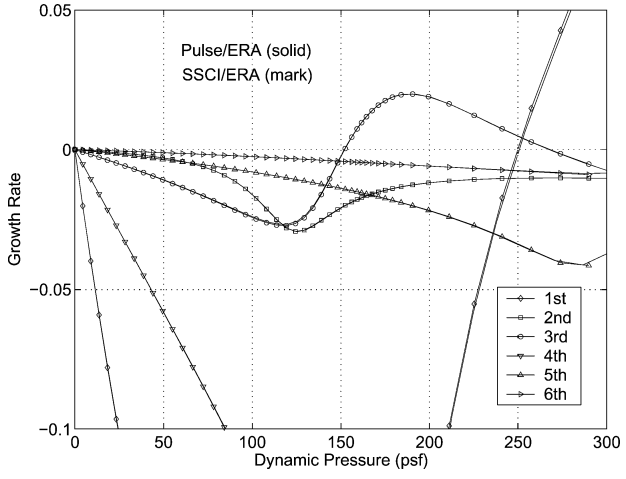

Fig. 22 V-g plot: SSCI/ERA (growth rate only).

Shown in Figs. 23 and 24 are transient aeroelastic responses of all of the ROMs in mode 1 and 2 due to an initial condition in mode 1. The two dynamic pressure values chosen for Figs. 23 and 24 represent a preflutter and the first instability points according to the pulse/ERA model. It is seen that the responses of the different ROMs generally match very well especially at the preflutter point with the responses of the pulse/ERA and SSCI/ERA ROMs being virtually identical to each other. However, the two ROMs based on FSCI/ERA show slight mismatches at $q = 152$ psf. In particular, the FSCI/ERA ROM 1 has not yet reached the flutter instability, whereas

Table 1 CFL3D CPU times required for ERAs

Method	CPU, h	Total no. of time steps
Pulse/ERA	366	9950
FSCI/ERA 1	79	1805
FSCI/ERA 2	79	2137
SSCI/ERA	64	1805

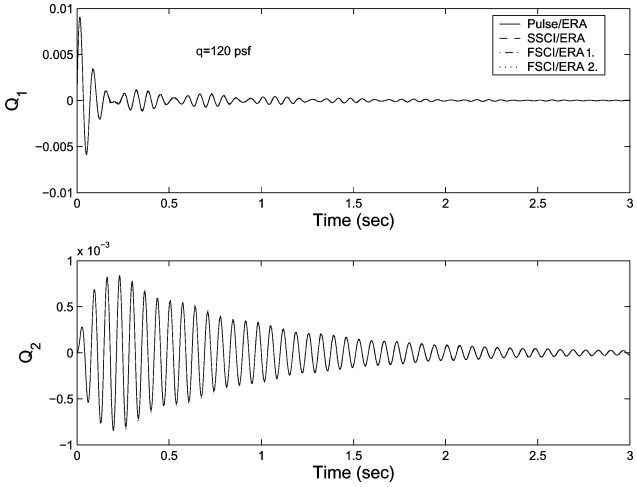

Fig. 23 Time history of aeroelastic responses due to the initial condition (IC) in mode 1 at $q = 120$ psf.

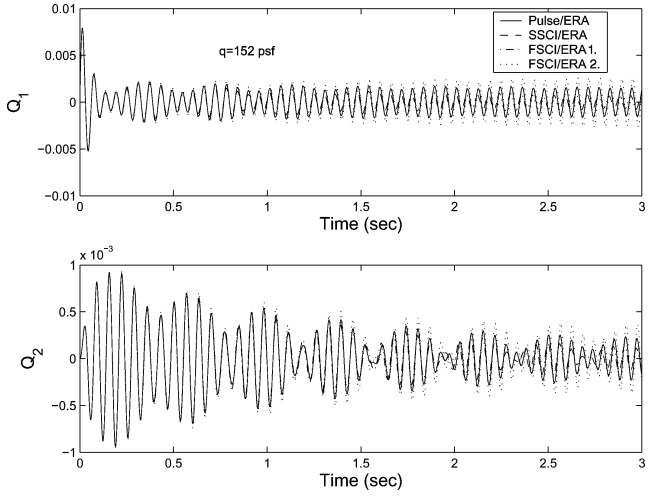

Fig. 24 Time history of aeroelastic responses due to IC in mode 1 at $q = 152$ psf.

the response of the FSCI/ERA ROM 2 is growing exponentially, all of which are well confirmed by the V–g plots presented earlier.

Comparison of Model Construction Times

Finally, the model construction time is compared between the different ERA ROMs. The model construction time here is defined as the CPU time elapsed during a CFL3D run in obtaining aerodynamic responses required by a specific ERA procedure. The time spent in the ERA postprocessing is not included because it is almost negligible compared to the CPU time spent by the CFL3D code. Table 1 shows the CPU hours measured on the IBM Regatta. From Table 1, it is clear that the new method has an advantage over the traditional pulse/ERA in reducing the computing time by a factor of 4–6. As shown in Ref. 15, it can be expected that the factor of saving will increase as more structural modes are added to the structural model.

Conclusions

This paper presented the new approach to generate the discrete-time, state-space CFD-based reduced-order aerodynamic and aeroelastic models for rapid flutter analysis at an affordable cost. The technique is based on the SCI/ERA that has recently been developed at Boeing. Because the SCI/ERA takes time samples mostly for a single representative input, rather than the multiple inputs individually, this process can significantly reduce the overall flow time of the model identification/reduction process.

The results presented were for the TETFM at Mach number 0.831 with 10 structural mode shapes and the unsteady flowfield modeled by the CFL3Dv6.0 code. Several types of signals including low-pass filtered and step input signals were considered for the simultaneous excitation of the flowfield, and the resulting time histories of the aerodynamic responses were used to generate the aerodynamic and aeroelastic ROMs in the state-space form. For comparison, a ROM based on the pulse/ERA was also generated using multiple pulse responses. From the various ROMs created, it was demonstrated that for the case of 10 inputs the new approach can save the computing time by a factor of 4–6 and still retain a high accuracy in the models. It is expected that this saving will increase as more structural modes are added to better describe the motion of the aircraft structure.

For future research, the following recommendations are made. First, more research needs to be done to define better input signals for various configurations. Second, the option to construct aerodynamic ROMs using extra aerodynamic measurements beyond the GAFs must be explored. In this case, it will be sufficient to sample the pulse responses only at the first two steps. Third, more research needs be done to define better input signals that can improve convergence of the CFD outputs without sacrificing the accuracy of the aerodynamic ROM especially in the low-frequency region. Finally, for completion of the process, it is desirable to optimize the number of time steps and automate the process.

Acknowledgment

The authors are grateful to Steven R. Precup, who continuously supported this research while he was the manager of the Methods Development Group.

References

[1]Schuster, D. M., Liu, D. D., and Huttsell, L. J., "Computational Aeroelasticity: Success, Progress, Challenge," *Journal of Aircraft*, Vol. 40, No. 5, 2003, pp. 843–856.

[2]Livne, E., "Future of Airplane Aeroelasticity," *Journal of Aircraft*, Vol. 40, No. 6, 2003, pp. 1066–1092.

[3]Roger, K. L., "Airplane Math Modeling and Active Aeroelastic Control Design," *Structural Aspects of Active Controls*, CP-228, AGARD, 1997, pp. 4.1–4.11.

[4]Karpel, M., "Design for Active Flutter Suppression and Gust Alleviation Using State-Space Aeroelastic Modeling," *Journal of Aircraft*, Vol. 19, No. 3, 1982, pp. 221–227.

[5]Karpel, M., and Hoadly, S. T., "Physically Weighted Approximations of Unsteady Aerodynamic Forces Using the Minimum-State Method," NASA TP 3025, 1991.

[6]Heimbaugh, R. M., "Flight Controls Structural Dynamics IRAD," McDonnell Douglas, Rept. MDC-J2303, March 1983.

[7]Winther, B. A., Goggin, P. J., and Dykman, J. R., "Reduced Order Dynamic Aeroelastic Model Development and Integration with Nonlinear Simulation," *Journal of Aircraft*, Vol. 37, No. 5, 2000, pp. 833–839.

[8]Thomas, J. P., Dowell, E. H., and Hall, K. C, "Three-Dimensional Transonic Aeroelasticity Using Proper Orthogonal Decomposition Based Reduced Order Models," *Journal of Aircraft*, Vol. 40, No. 3, 2003, pp. 544–551.

[9]Kim, T., "An Efficient Response-Based Modal Analysis for Dynamic Systems with Multiple Inputs," AIAA Paper 2001-1380, April 2001.

[10]Kim, T., and Bussoletti, J. E., "An Optimal Reduced-Order Aeroelastic Modeling Based on a Response-Based Modal Analysis of Unsteady CFD Models," AIAA Paper 2001-1525, April 2001.

[11]Silva, W. A., and Raveh, D. E., "Development of Unsteady Aerodynamic State-Space Models from CFD-Based Pulse Responses," AIAA Paper 2001-1213, April 2001.

[12]Silva, W. A., and Bartels, R. E., "Development of Reduced-Order Models for Aeroelastic Analysis and Flutter Prediction Using the CFL3Dv6.0 CFD Code," *Journal of Fluids and Structures*, Vol. 19, No. 6, 2004, pp. 729–745.

[13]Hong, M. S., Bhatia, K. G., SenGupta, G., Kim, T., Kuruvila, G., Silva, W. A., Bartels, R., and Biedron, R., "Simulations of a Twin-Engine Transport Flutter Model in the Transonic Dynamics Tunnel," International Forum on Aeroelastic and Structural Dynamics, IFASD Paper 2003-US-44, June 2003.

[14]Juang, J.-N., and Pappa, R. S., "Eigensystem Realization Algorithm for Modal Parameter Identification and Model Reduction," *Journal of Guidance, Control, and Dynamics*, Vol. 8, No. 5, 1985, pp. 620–627.

[15]Kim, T., "Efficient Reduced-Order System Identification for Linear Systems with Multiple Inputs," *AIAA Journal*, Vol. 43, No. 7, 2005, pp. 1455–1464.

[16]Papoulis, A., *Probability, Random Variables, and Stochastic Processes*, McGraw–Hill, New York, 1982, Chap. 8.

[17]Kim, T., "Frequency-Domain Karhunen–Loeve Method and Its Application to Linear Dynamic Systems," *AIAA Journal*, Vol. 36, No. 11, 1998, pp. 2117–2123.

[18]Kim, T., "Discrete-Time Eigen Analysis and Optimal Model Reduction for Flutter & Aeroelastic Damping/Frequency Prediction Based On CFL3D-ERA," Boeing Commercial Airplane Group, B-ADVTECH-LLL-M02-013, Seattle, WA, Feb. 2003.

[19]SenGupta, G., Seidel, D. A., Young, D. P., and Bussoletti, J. E., "Effect of Wind Tunnel Walls on the Flutter Characteristics of an Airplane Model," AIAA Paper 2001-1655, April 2001.

A. Berman
Associate Editor